Talanta 228 (2021) 122060

Contents lists available at ScienceDirect

Talanta

journal homepage: www.elsevier.com/locate/talanta

Porphyrin-based covalent organic framework as bioplatfrom for detection of vascular endothelial growth factor 165 through fluorescence resonance energy transfer

Jing Cui, Lun Kan, Zhenzhen Li, Longyu Yang, Minghua Wang, Linghao He, Yafei Lou, Yulin Xue, Zhihong Zhang *

School of Materials and Chemical Engineering, Zhengzhou University of Light Industry, No. 136, Science Avenue, Zhengzhou, 450001, China

ARTICLE INFO

Keywords:
Porphyrin-based covalent-organic framework
Fluorescence aptasensor
Detection of vascular endothelial growth factor 165
Carbon dots

ABSTRACT

A fluorescent aptasensor based on porphyrin-based covalent organic framework (p-COF) and carbon dots (CDs) was constructed for detecting vascular endothelial growth factor 165 ($VEGF_{165}$) and for imaging of the breast cancer cell line Michigan cancer foundation-7 (MCF-7). CDs synthesized with strong photoluminescence at λ~380 nm were used as donors to label the $VEGF_{165}$-targeted aptamers (Apt_{VEGF}/CDs). Additionally, the p-COF nanostructure comprised rich functional groups of C═N on the surface and π-stacking planar nanostructure, resulting in the CDs adsorption via weakly π−π stacking, hydrogen bond and the Van der Waals force. Thereby, the fluorescence resonance energy transfer (FRET) occurred due to the close distance between the p-COF network and CDs, leading to the quenching of the fluorescence feature of CDs and p-COF. In the presence of $VEGF_{165}$, the G-quadruplex was formed via the specific binding between $VEGF_{165}$ and aptamer. It impelled that the release of partial $VEGF_{165}$-Apt_{VEGF}/CDs complex, affording the fluorescence recovery of the sensing system to some extent. Consequently, the proposed Apt_{VEGF}/CDs/p-COF fluorescence biosensor offered excellent analytical performances for the $VEGF_{165}$ detection, displaying a detection limit of 20.9 fg mL^{-1} within a wide linear range of the $VEGF_{165}$ concentration of 1.0 pg mL^{-1}–100 ng mL^{-1}. The developed fluorescence biosensor was also used to determine $VEGF_{165}$-overexpressed in MCF-7 cancer cells. Thereby, the present work can greatly widen the application of COFs in the development of aptasensors and cancer diagnosis.

1. Introduction

Aptamer biosensors, which are based on the specific recognition between aptamer strands and corresponding targets, have been explored for early detection of various tumor biomarkers [1,2] and living cancer cells [3,4] owing to their high sensitivity, good selectivity, fast response, and low cost [5]. As an important biomarker, vascular endothelial growth factor (VEGF) indicates different diseases including breast cancer, lung cancer, colorectal cancer, and rheumatoid arthritis [6–8]. Four different species, namely, $VEGF_{121}$, $VEGF_{165}$, $VEGF_{189}$, and $VEGF_{206}$, can be formed through alternative exon splicing. Among them, $VEGF_{165}$, generated in the absence of the residue encoded by exon 6 [9,10], is often overexpressed in cancer cells during tumor growth. In this regard, rapid and efficient $VEGF_{165}$ detection is essential for early diagnosis and treatment. Various detection and quantification methods have been developed for rapid determination of $VEGF_{165}$ including enzyme-linked immunosorbent assays (ELISA) [11,12], fluorescent methods [13–15], surface-enhanced Raman scattering [16], electrochemiluminescence [17], and electrochemical techniques [18,19]. However, these techniques often require sophisticated instrumentation with complicated protocols, which make them expensive, labor intensive, time consuming, thereby restricting their widespread application in real-time clinical diagnoses. Therefore, the development of rapid, highly sensitive and selective, cost-effective, and label-free methods for detection of $VEGF_{165}$ in blood/serum is of great significance for clinical diagnosis, fundamental research, and drug discovery.

Recently, the development of fluorescence methods has received considerable attention owing to equipment simplicity, free separation, and fast response [20–22]. The excellent performance and good biocompatibility of donor–acceptor pairs are two significant factors used to improve the efficiency of fluorescence resonance energy transfer (FRET) and analytical performance [23]. Various nanomaterials

* Corresponding author.
E-mail address: 2006025@zzuli.edu.cn (Z. Zhang).

https://doi.org/10.1016/j.talanta.2020.122060
Received 14 October 2020; Received in revised form 19 December 2020; Accepted 23 December 2020
Available online 30 December 2020

including quantum dots (QDs) [24,25], nanoparticles [26], organic dyes, carbon nanotubes [23] have been applied to modify probe molecules for construction of FRET sensing strategies. Due to the lack of water dispersibility, poor biocompatibility, high cytotoxicity, or complicated preparation methods, however, further applications of these materials in the fields of biosensors are remarkably limited. Therefore, seeking of benign alternatives has become increasingly important and urgent. The carbon dots with nanosize recently emerge as superior fluorophores with their merits, including excellent photostability, small size, biocompatibility, ease to be functionalized with biomolecules and chemical inertness [27,28].

As an emerging class of ordered crystalline porous polymers, covalent–organic frameworks (COFs) are constructed from light elements and connected with organic monomers by strong covalent bonds [29,30]. Many research demonstrate that COFs can be widely used in various fields, including gas storage, catalysis, microbiology, disease therapy, sensors, and chromatographic separation [31–33], because of their comparable surface areas, ordered channel structures, well-defined pore apertures, thermal stability, and chemical stability. COFs-based nanomaterials exhibit strong immobilization ability toward some probes, namely, DNA aptamer strands or antibodies, via π-stacking interaction, hydrogen bonds, and electrostatic interaction. In this regard, COFs can be explored as anchored platforms of biosensors [34,35], such as two-dimensional porphyrinic-COF for label-free detection of C-reactive protein [34], Py-M-COF immobilized with DNA aptamer strand to sensitively detect different antibiotics [35], and COF DHTA-TTA for electrochemical sensing [36]. Apart from the applications of COFs as platforms of biosensors, they can be further used as scaffolds for fluorescent probes owing to their strong fluorescence performance [37]. Ding et al. [38] fabricated a thioether-functionalized COF for fluorescence detection and removal of mercury (II). Zhang et al. synthesized a fluorescence PI-COF and utilized it as a fluorescent probe for analyzing 2,4,6-trinitrophenol [39]. In these works, the fluorescence can be quenched upon metal–ligand coordination or extended π-conjugation interaction with targets via donor–acceptor energy and charge transfer [37]. In other words, these fluorescence sensors employ the fluorescence change of COFs with analytes to realize fluorescence turn-off detection, thereby show drawbacks such as high background and low sensitivity compared to fluorescence turn-on sensors [40,41]. Furthermore, the selectivity of these COF-based sensing strategies is also limited due to the lack of specific recognition groups toward the target analysts [41,42]. Therefore, novel sensitive and selective COFs-based turn-on biosensors are highly promising. In this regard, COFs not only can act as the sorbent to adsorb the probe but also can used as accepter to quench the fluorescence of the probe. For example, a COFs-based fluorescent turn-on platform was fabricated for sensing biomolecules [37]. The layered structure TPA-COF was employed as a fluorescent sensing platform for sensitive detection of DNA [43]. Nonetheless, the exploration of fluorescent aptasensors for detecting $VEGF_{165}$ based on COFs is still in its early stage, especially for applications in early diagnosis of cancer cells overexpressing $VEGF_{165}$.

In this work, we designed and constructed a sensitive and selective fluorescent turn-on aptasensor for detection of $VEGF_{165}$. A pair of fluorescence indicators including p-COF and biocompatible CDs modified with the $VEGF_{165}$-targeted aptamer were separately prepared. Amongst, CDs were synthesized through controlled thermal pyrolysis of citric acid and urea, showing excellent biocompatibility, rich carboxyl groups, and strong fluorescence. Therefore, CDs can be used as both the indicator after modifying the amino-functionalized aptamer [44] and the accepter to quench the fluorescence via FRET [45]. Additionally, p-COF network was synthesized via the covalent binding of 5,10,15,20-tetra (4-aminophenyl) porphyrin (TAPP) and 1,10-phenanthroline-2,9- dimethylaldehyde (PDA) (Scheme 1), comprising rich of functional groups of C═N and planar π-π stacking network structure on surface and strong fluorescence emission. Thus, it was used as the platform for anchoring Apt_{VEGF}/CDs and the fluorescence donor. Compared with other fluorescence aptasensors, the developed p-COF--based sensor displayed an ultra-low limitation of detection (LOD) of

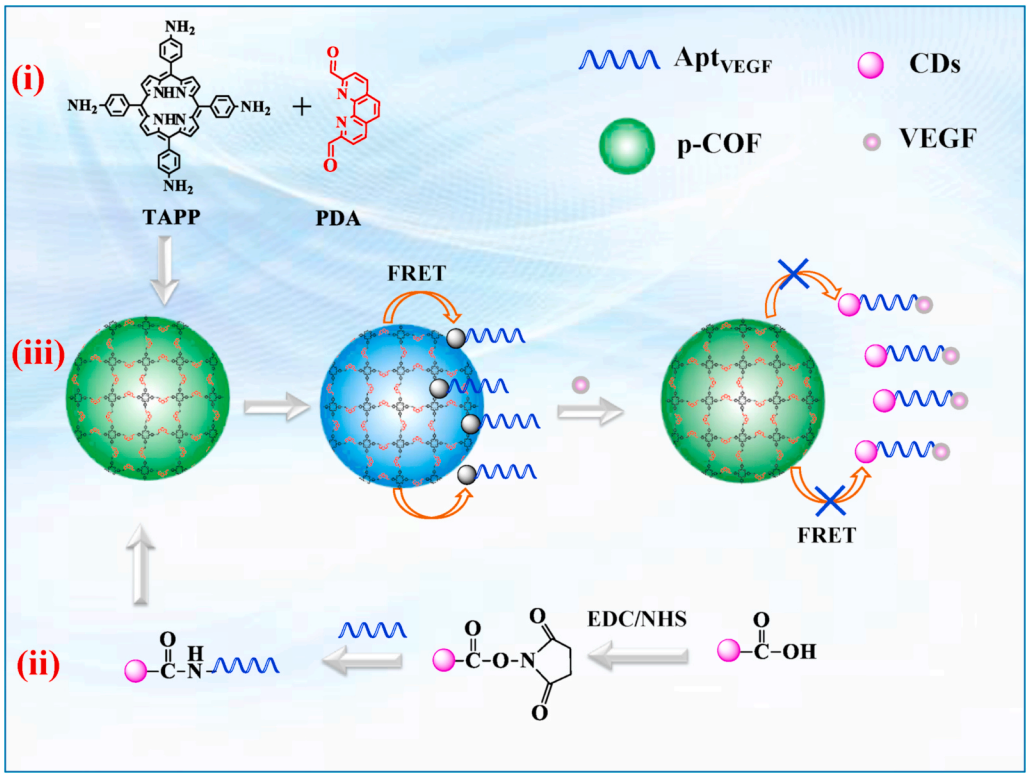

Scheme 1. Schematic representation of p-COF-based fluoresce biosensor, including: (i) The synthesis route of the p-COF network, (ii) the preparation procedure of CDs and Apt_{VEGF}/CDs complex, (iii) the principle of the proposed biosensor based on p-COF for detection of $VEGF_{165}$.

20.9 fg mL^{-1} toward $VEGF_{165}$ within a range of 1.0 fg mL^{-1}-100 ng mL^{-1}. The sensor also exhibited good selectivity, stability, reproducibility, and acceptable applicability. Furthermore, the proposed p-COF-based fluorescence aptasensor was applied to detect living MCF-7 cancer cells, which overexpress $VEGF_{165}$ [46].

2. Experimental section

The parts of materials and reagents, the preparation methods of all solutions, preparation of CDs, analysis of surface morphology and structure characterization, and fluorescence measurements are provided in the SI (See the Supplementary Material).

2.1. Synthesis of p-COF

As illustrated in Scheme 1 (Part i), the p-COF network was synthesized through the solvothermal method [47]. PDA (0.08 mmol, 18.9 mg) and TAPP (0.04 mmol, 25.8 mg) were dissolved in the mixed solvent of 20 mL of ethanol 20 mL of 1,3,5-trimethylbenzene mixture solvent, for which 0.2 mL acetic acid was used as catalyst. After ultrasonic for 20 min, the synthesis system was further reacted at 120 °C for 72 h. Subsequently, the product was washed several times with 1,3,5-trimethylbenzene and ethanol, separately, and dried at 60 °C in vacuum for further 12 h.

2.2. Preparation of the Apt_{VEGF}/CDs complex

As illustrated in Scheme 1 (Part ii), carboxyl group bearing on the synthesized CDs was firstly esterified to ester group using N-Hydroxysuccinimide (NHS) and 1-(3-dimethylaminopropyl)-3- ethylcarbodiimide hydrochloride (EDC) [48] in 10 mL of phosphate buffer solution (PBS) (pH 7.4) containing 1 mM NHS and 4 mM EDC at 4 °C for 2 h [40]. After washed with Milli-Q water and dried under a N_2 stream, (5 mg) CDs modified with activated ester group was dispersed in 10 mL of PBS. Subsequently, the CD dispersion was mixed with the Apt_{VEGF} solution (100 nM, 10 mL) and stored at 4 °C for 12 h. During this period, the aptamer strands modified with amino group can be covalently anchored onto the esterified CDs by the formation of amide bond [44] (represented by Apt_{VEGF}/CDs). Afterward, the dispersion was filtered and collected, following by washing by Milli-Q water for three times. The obtained Apt_{VEGF}/CDs powder was dispersed in 10 mL PBS again and stored in a refrigerator (4 °C) for further use.

2.3. Construction of the p-COF-based fluorescent biosensor for the detection of $VEGF_{165}$

According to the manufacture of the p-COF-based fluorescent aptasensor, the p-COF powder (2 mg) was dispersed into 10 mL of PBS solution (pH 7.4), forming the homogeneous dispersion. Afterward, the p-COF dispersion (1 mL) was added into the Apt_{VEGF}/CDs suspension (1 mL, 2 mg mL^{-1}), following by being mixed evenly and stored in a refrigerator at 4 °C for 4 h and centrifuged to obtain the supernatant (represented by Apt_{VEGF}/CDs/p-COF). Subsequently, the resultant sample was added 1 mL of $VEGF_{165}$ solution (1.0 ng mL^{-1}), evenly mixed and stored at 4 °C for 2 h (denoted as VEGF/(Apt_{VEGF}/CDs)/p-COF).

The LOD of the p-COF-based fluorescence biosensor was performed by measuring the fluorescence properties of the Apt_{VEGF}/CDs/p-COF suspension (2 mg mL^{-1}) after adding the series of $VEGF_{165}$ solutions with various concentrations ranging of 0.001, 0.01, 0.1, 1.0, 10, 100 and 200 ng mL^{-1}. Upon analysis of the fluorescence intensity of the system as a function of the $VEGF_{165}$ concentration, a regression equation manifesting the relationship between the fluorescence intensity and $VEGF_{165}$ concentration was plotted, through which the LOD and the dynamic range were obtained.

The selectivity of the proposed sensor toward $VEGF_{165}$ was conducted by measuring the fluorescence intensity of the Apt_{VEGF}/CDs/p-COF suspension in the presence of potentially interferents, including alpha Fetoprotein (AFP), carcinoembryonic antigen (CEA), MUCl protein-1 (MUC1), protein tyrosine kinase7 (PTK7), prostate specific antigen (PSA), human epidermal growth factor receptor-2 (HER2), and bovine serum albumin (BSA), along with their mixed solution. The concentration of the used interferent suspension was 100 ng mL^{-1} which was 100-folds larger than that of the $VEGF_{165}$ solution.

The reproducibility of the fabricated p-COF-based aptasensor was further validated by testing the fluorescence intensities of five parallel $VEGF_{165}$/(Apt_{VEGF}/CDs)/p-COF dispersions prepared by the same procedure. The fluorescence signal of each measurement was recorded and plotted for comparison.

The storage stability of the fabricated biosensor was evaluated by continuously measuring the fluorescence intensity of the $VEGF_{165}$/(Apt_{VEGF}/CDs)/p-COF suspension. Specifically, the $VEGF_{165}$/(Apt_{VEGF}/CDs)/p-COF suspension (2 mg mL^{-1}) was stored in a refrigerator at 4 °C for 15 days. During this period, its fluorescence intensity was measured daily, following by analyzing the change of fluorescence intensity.

2.4. Cell cytotoxicity and cell imaging

Cell cytotoxicity of fabricated-COF-based fluorescence aptasensor was performed by using a microplate reader (Thermo Fisher Scientific, Inc., U.S.A.). Cellular uptake and distribution inside cellular were further investigated by using a confocal laser scanning microscopy (CLSM, LSM710, ZEISS, Germany) excited at 480 nm.

The in *vitro* cytotoxicities of p-COF, Apt_{VEGF}/CDs and (Apt_{VEGF}/CDs)/p-COF were quantified by the 3-(4,5-dimethylthiazol-2-yl)-2,5-diphenyltetrazolium bromide (MTT) assay. The MCF-7 cancer cells and L929 normal cells were cultured in 96-cell plates with 8000 cells per well (density 8000 cells well^{-1}) for 24 h respectively. After that, L929 and MCF-7 cells were separately treated with p-COF and (Apt_{VEGF}/CDs)/p-COF in Dulbecco's modified Eagle medium (DMEM) and continuously incubated for another 24 h. Subsequently, cells were moved from the medium and washed twice by PBS to remove possible material, and further incubating with fresh DMEM for 2 days. Afterward, 20 μL of MTT (5 mg mL^{-1}) and 150 μL of dimethyl sulfoxide were added into per well. Then, the plates were shaken for 15 min to dissolve the purple crystals. The cytotoxicity was calculated by measuring the absorbance at 490 and 630 nm with a microplate reader.

For the investigation of cell imaging, living MCF-7 and L929 cells (density 1×10^5 cells well^{-1}) were seeded in a laser confocal culture dish and incubated at 37 °C with 5% CO_2 for 12 h. Then the cells were further incubated with new medium containing Apt_{VEGF}/CDs/p-COF (50 μg mL^{-1}) for 1 h, and washed by PBS. At last, cells were fixed with 4% paraformaldehyde (Hoechst 33342 (300 nM)) for 15 min at 37 °C. Cells images were characterized by a CLSM with HeNe laser excitation source at 370 nm.

2.5. Real samples

To test the practicability of the proposed fluorescence biosensor, human serum sample was used which was obtained from the First Affiliated Hospital of Zhengzhou University after permission and informed consent of the patient. Moreover, the experimental protocol was conformed to the ethical standards of the 1964 Declaration of Helsinki and its later amendments. It was approved by the ethics committee of the First Affiliated Hospital of Zhengzhou University. After the whole blood was collected, it was left at room temperature for 0.5 h and centrifuged at 2000 r min^{-1} for 10 min. The resultant supernatant serum was separated and stored at −20 °C. The $VEGF_{165}$ solutions with diverse concentrations (0.001, 0.01, 0.1, 1, 10, 100 and 200 ng mL^{-1}) were separately spiked into the human blood serum samples. The real concentration of $VEGF_{165}$ concentration was determined using the present fluorescence biosensor. The feasibility for clinical diagnosis was

evaluated by comparing the used concentration and the calculated concentration according to the regression equation.

3. Results and discussion

3.1. Basic characterization of CDs and the Apt_{VEGF}/CDs complex

As demonstrated in Fig. S1a, the synthesized CDs exhibit near-spherical morphology with diameter ranging from 4 nm to 10 nm. The FTIR (Fig. S1b) and XPS (Figs. S1c-f) results indicate that the synthesized CDs possess large number of hydrophilic groups, such as C–N, C═O, $–NH_2$, and –OH, which cannot only significantly improve the hydrophilicity and stability of CDs in aqueous system without modification but also can provide abundant action sites for adsorption on the p-COF surface via diverse weak interaction. The detailed description and discussion of the basic characteristics of CDs are supplied in the S2 part (See the Supplementary Material). Changes in the chemical structure of CDs before and after the adsorption of aptamer strands (Apt_{VEGF}/CDs) were characterized by XPS to evaluate whether the strands can be immobilized with CDs. As displayed in Figs. S2a-d, apart from C═C, C–C, C–O, C═O, and COOH groups, the appearance of C–N and N–C═O with high peak intensities can be observed, which originated from the oligonucleotide strands. Furthermore, the strong N 1*s* XPS spectrum (Fig. S2b) can be separated into four components including pyridinic N (398.1 eV), C–N/N–H (399 eV), O═C–N–C═O (399.6 eV), and N–O (401.1 eV), which are due to the base ring on the aptamer sequence. The presence of the N–C═O group reveals the successful binding of aptamer strands to CDs by covalent bond.

3.2. Basic characterization of the p-COF network

The surface morphology of p-COF (Figs. S3a-d) indicates the spherical particles with diameter around 100 nm. The high-resolution TEM image (Fig. 1a and b) suggests that the p-COF nanostructure is composed of several flake and layered structures, which are aggregated by several layers due to π-stacking and hydrogen bonding interaction [49]. The crystal structure, chemical composition, and fluorescence performance of p-COF were investigated by XRD, FT-IR, and fluorescence spectrum analyses, respectively. As shown in Fig. S3e, diffraction peaks located $2\theta = 18^\circ$ and 20.16° can be observed in the XRD pattern of p-COF, implying the preferred stacking structure and the semi-crystalline nature. Fig. 1c shows the FT-IR spectrum of p-COF and the investigation of raw materials of TAPP and PDA for comparison. p-COF and TAPP show strong absorption bands located at 3316 and 1702 cm^{-1}, which are assigned to the stretching and bending vibration of N–H bonds, respectively. This finding indicates the involvement of TAPP during the reaction. The absorption peak at 1619 cm^{-1} observed for p-COF arises from the stretching band of C═N [43], confirming the successful formation of imine linkage. The peak located at ~1685 cm^{-1} for PDA corresponds to the attenuation of the stretching vibration of the aldehyde band; this finding indicates the formation of imine-linked bonds between TAPP and PDA [43]. Moreover, the Raman spectrum of p-COF

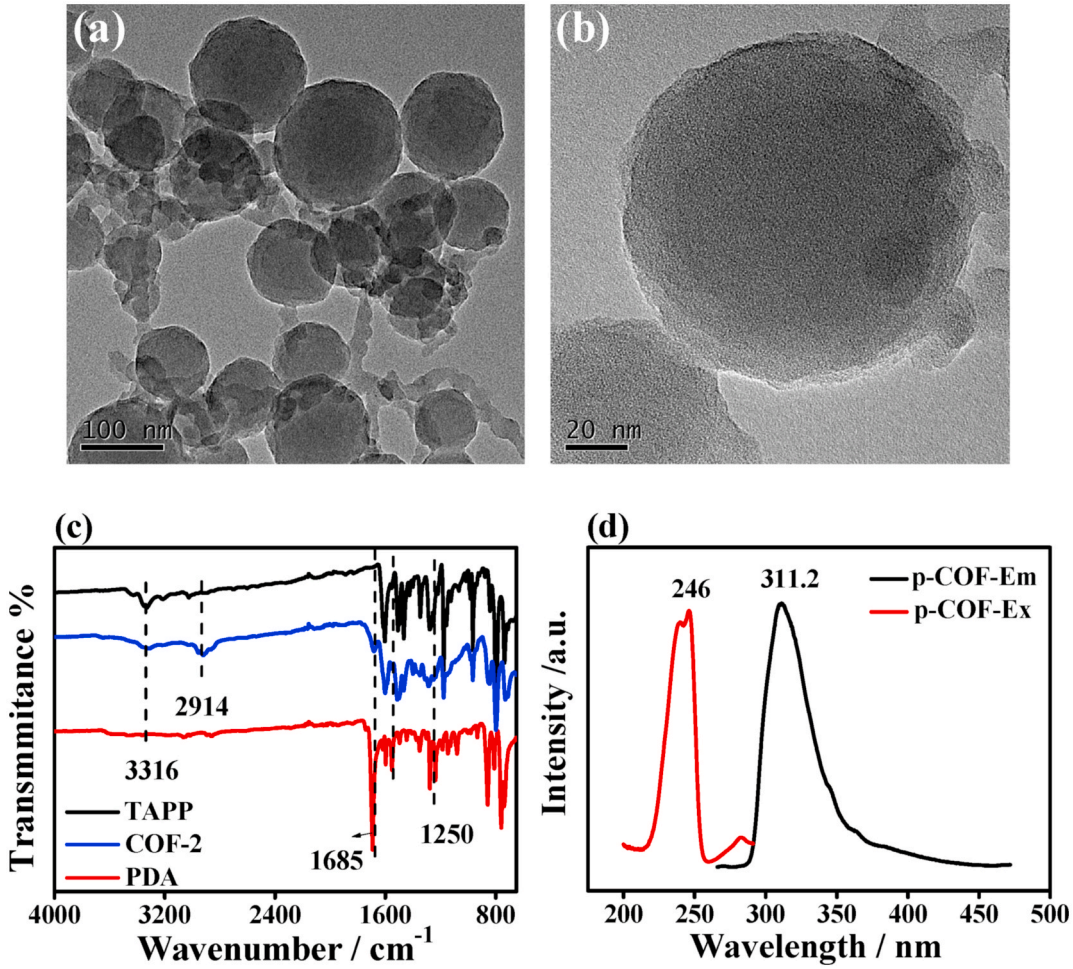

Fig. 1. (a, b) Low- and high-magnification TEM images, (c) FTIR spectrum and (d) fluorescence spectrum of the synthesized p-COF (In Fig. 1c, reactants including TAPP (black line) and PDA (red line) were displayed for comparison. (For interpretation of the references to color in this figure legend, the reader is referred to the Web version of this article.)

(Fig. S3f) exhibits two clear characteristic peaks at 1335 and 1560 cm^{-1}, which attributed to D and G bands, respectively. The ratio of the intensities of D and G bands (I_D/I_G) is about 0.89, indicating the definite structural defects and carbon-rich nanostructure of p-COF. In addition, the fluorescence spectrum of p-COF (Fig. 1d) shows clear and strong fluorescence intensity with the excitation maxima peak at approximately 246 nm and the emission maximum at approximately 311 nm. This finding reveals the possibility of exploring p-COF as a novel bioplatform for fluorescence aptasensors [50].

The XPS survey scan spectrum of p-COF reveals that it is composed of C 1*s* (284.6 eV) and N 1*s* (400 eV) signals. The chemical structure and valence state of C 1*s* and N 1*s* are illustrated in Fig. 2a–b. The high-resolution C 1*s* XPS spectrum (Fig. 1a) is separated into three main peaks at binding energy (BE) levels of 283.8, 284.4, and 285.1 eV, which correspond to C═C, C–C, and C–N, respectively. The large content of the C═C group indicates the highly conjugated structure of p-COF. This finding reveals the π−π stacking interaction when in contact with CDs. The three other weak peaks at BE levels of 286.9, 288.9, and 291.6 eV are due to C═O, N–C═O, and π−π* bonds. The presence of oxygen-related groups originate from oxygen contamination during the XPS measurement. In the high-resolution N 1*s* XPS spectrum (Fig. 1b), three fitted major peaks at BE levels of 397.2, 398.5, and 399.3 eV are assigned to –N=, –N–, and N–$(C)_3$ or H–N–$(C)_2$ bonds, respectively. The two other peaks at BE levels of 400.1 and 401.8 eV correspond to NH_2 and graphitic N on p-COF. All these results suggest that the p-COF displays amorphous graphene-like structure and strong fluorescence performance and contains abundant chemical groups. Hence, the p-COF demonstrates potential as a novel platform for fluorescence biosensors.

Whether the Apt_{VEGF}/CDs complex can be immobilized over the p-COF matrix should be checked to assess the biosensing performance of the proposed p-COFs-based aptasensor. XPS characterization of the binding of the p-COF to the Apt_{VEGF}/CDs complex was conducted to analyze the difference before and after the adsorption. The high-resolution C 1*s*, N 1*s*, P 2*p*, and S 2*p* XPS spectra of Apt_{VEGF}/CDs/p-COF is shown in Fig. 2c–f. In comparison with the C 1*s* XPS spectrum of the pristine p-COF (Fig. 2a), the peak intensities of C═O, N–C═O, and COO groups on p-COF/Apt_{VEGF}/CDs are higher (Fig. 2c). This finding implies the presence of aptamer strands over the COF network. Additionally, four peaks of -N-, N-$(C)_3$ or H–N-$(C)_2$, NH_2, and graphitic N appear the N 1*s* XPS spectrum of the p-COF/Apt_{VEGF}/CDs complex (Fig. 2d). Only the surface chemical structure of the p-COF/Apt_{VEGF}/CDs complex can be determined given that the limitation thickness of the XPS characterization is only 8–10 nm [51]. The disappearance of the –N= group indicates the full coverage of the Apt_{VEGF}/CDs complex on the p-COF surface. Furthermore, the presence of the p 2*p* signal (Fig. 2c) confirms the presence of aptamer strands. The remarkable S *2p* signal

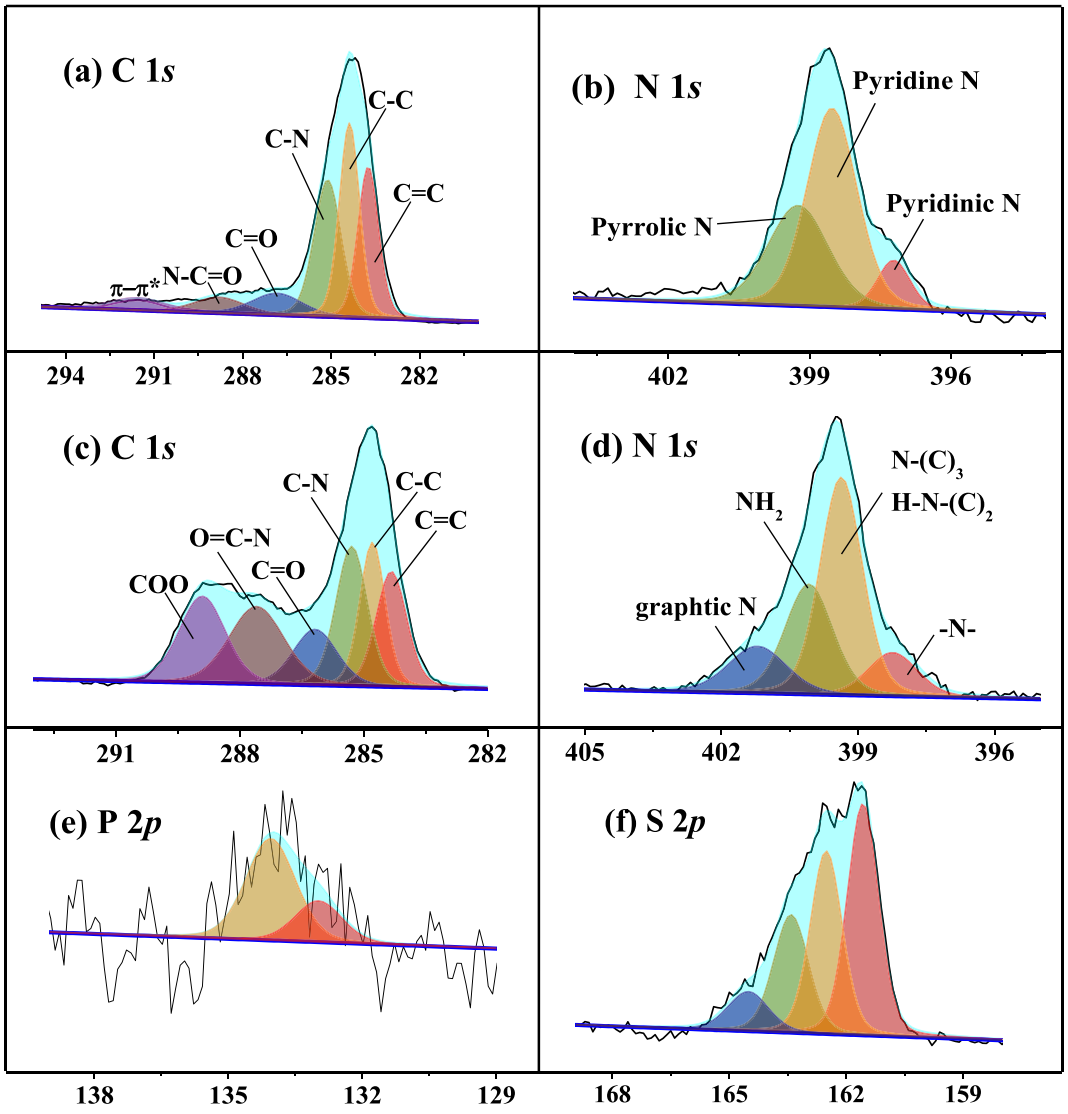

Fig. 2. High-resolution of XPS spectra (a) C 1*s* and (b) N 1*s* for p-COF, and (c) C 1*s*, (d) N 1*s*, (e) P *2p*, (f) S *2p* of p-COF/Apt_{VEGF}/CDs.

originates from CDs (Fig. 2d), revealing the presence of CDs of the p-COF/Apt_{VEGF}/CDs complex. These results reveal the successful anchoring of the Apt_{VEGF}/CDs complex over the p-COF layer, which can be further used to detect the corresponding target, namely, $VEGF_{165}$.

3.3. Working principle of the p-COF-based biosensor

As illustrated in Scheme 1, the CD surface was modified with the $VEGF_{165}$-targeted aptamer, which specifically recognizes $VEGF_{165}$ via the formation of the G-quadruplex between them, forming the Apt_{VEGF}/CDs complex. Meanwhile, the proposed p-COF demonstrated the extended strong planar π-electron system and N structure and thus can adsorb the Apt_{VEGF}/CDs complex via hydrogen bonding [43], Van der Waals force [52] and π-π stacking interaction [37,53]. The close distance between p-COF and the Apt_{VEGF}/CDs complex substantially leads to the quenched fluorescence of CDs via FRET [52,54]. In the presence of $VEGF_{165}$, the specially recognized binding between aptamer and $VEGF_{165}$ impels the aptamer strands to bind with $VEGF_{165}$. This kind of binding interaction is stronger than that of the adsorption ability between the Apt_{VEGF}/CDs complex and p-COF. As such, the Apt_{VEGF}/CDs complex easily detaches from the p-COF matrix. Along with the enlargement of the distance between CDs and p-COF matrix, the

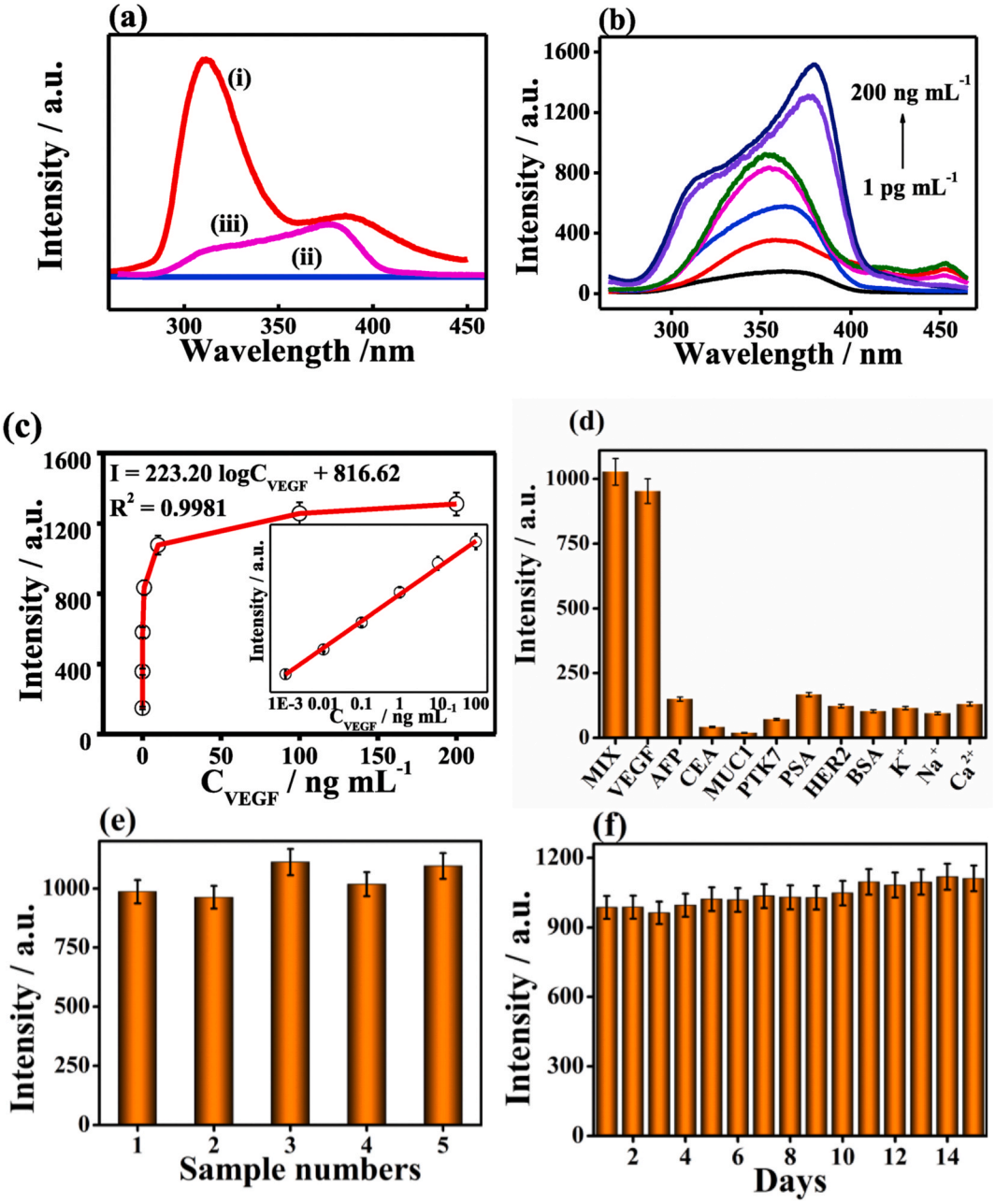

Fig. 3. (a) Fluorescence signals of the COF-based aptasensor during the construction process, including (i) p-COF, (ii) p-COF/Apt_{VEGF}/CDs, and (iii) $VEGF_{165}$/p-COF/Apt_{VEGF}/CDs. (b) The fluorescence intensities of the p-COF/Apt_{VEGF}/CDs by incubating with the $VEGF_{165}$ concentration with various concentrations. from bottom to top: 1 pg mL^{-1}, 10 pg mL^{-1}, 100 pg mL^{-1}, 1 ng mL^{-1}, 10 ng mL^{-1}, 100 and 200 ng mL^{-1}. (c) The corresponding relationships between the fluorescence intensity and the $VEGF_{165}$ concentrations from 1 pg mL^{-1} to 100 ng mL^{-1}. The inset shows the linear relationship between ΔI/I and the concentration of $VEGF_{165}$. (d) Selectivity of p-COF-based fluorescence aptasensor for detecting diverse interferwents, including BSA, HER2, PSA, PTK7, MUC1, CEA, AFP (1 μg mL^{-1}), and their mixture with $VEGF_{165}$. (e) Reproducibility of the p-COF-based fluorescence aptasensor for detecting $VEGF_{165}$ (10 ng mL^{-1}). (f) Stability of the p-COF-based aptasensor for $VEGF_{165}$ detection (10 ng mL^{-1}).

fluorescence of CDs can be recovered and becomes intense [37]. The recovery efficiency of the fluorescence signal of CDs is dependent on the amount of $VEGF_{165}$ in the aqueous solution. By taking advantages of bi-color FRET from donors to acceptor and target-induced fluorescence recovery, VEGF can be simultaneously quantified according to the linear increase in the recovered fluorescence intensity with biomarker concentration [37].

3.4. Detection of $VEGF_{165}$ with p-COF-based biosensor

Fluorescence signals during the construction of the COFs-based aptasensor, including pristine p-COF, p-COF/Apt_{VEGF}/CDs, and $VEGF_{165}$/p-COF/Apt_{VEGF}/CDs, were acquired through fluorescence spectroscopy to assess the feasibility of the proposed p-COF-based aptasensor (Fig. 3a). p-COF nanospheres exhibit strong fluorescence at 311 nm. After adding the Apt_{VEGF}/CDs complex into the p-COF dispersion, negligible fluorescence signal was observed. The FRET effect occurred between the Apt_{VEGF}/CDs complex and the p-COF layer. Previous work proved that the p-COF displays large surface area and a porous and highly conjugated structure. The Apt_{VEGF}/CD complex can bind to the COF layer via π−π stacking and hydrogen bonds [55], for which the FRET effect occurs, quenching the fluorescence performance of CDs. When adding the $VEGF_{165}$ solution into the system, the fluorescence intensity increases at 370 nm. Given the recognition interaction between the aptamer strands and $VEGF_{165}$, a G-quadruplex structure was formed, leading to the rapid detachment of Apt_{VEGF}/CDs from the p-COF matrix. As a result, the quenched fluorescence of the COF-based biosensor was rapidly recovered. The rapid adsorption and detachment of Apt_{VEGF}/CDs from the p-COF matrix confers the use of the designed COF-based biosensor for fluorescence determination of $VEGF_{165}$.

The experimental parameters for the detection of $VEGF_{165}$ were optimized to obtain superior sensing performance, as displayed in the S4 part (See the Supplementary Material). The effect of the concentration of p-COF on the sensing performance was investigated primarily within the p-COF concentration of 0.5–5 mg mL^{-1}. The fluorescence intensity of the $VEGF_{165}$/p-COF/Apt_{VEGF}/CDs solution increases when the p-COF concentration is less than 2 mg mL^{-1}. Numerous $VEGF_{165}$ molecules combine with the aptamer, resulting in the release of $VEGF_{165}$/Apt_{VEGF}/CDs complexes from the p-COF matrix and the partial recovery of the fluoresce performance of CDs. Afterward, the intensity substantially decreases with further increase in the concentration (Figs.S4a-b). When excessive $VEGF_{165}$/Apt_{VEGF}/CDs complexes are present in the aqueous solution, the self-quenching of fluorescence among the complexes would occur, thereby decreasing the fluorescence intensity again. Therefore, the optimal p-COF concentration for determination of $VEGF_{165}$ was chosen as 2 mg mL^{-1}. Moreover, the effect of the aptamer concentration on the sensing performance was investigated within 20–300 nM. As shown in Figs. S4c-d, the fluorescence intensity of the $VEGF_{165}$/p-COF/Apt_{VEGF}/CDs solution increases to the maximum at the VEGF aptamer concentration of 100 nM. After that, the intensity remains stable with further increase in the aptamer concentration. This finding indicates the saturated anchoring of the aptamer strands at 100 nM. Therefore, the aptamer with concentration of 100 nM was chosen for subsequent experiments.

In the proposed sensing strategy, the quantitative behavior of the developed fluorescence techniques for detecting $VEGF_{165}$ was analyzed under the optimum conditions. As demonstrated in Fig. 3a–b, the fluorescence spectra of the $VEGF_{165}$/p-COF/Apt_{VEGF}/CDs solution were recorded along with the concentration of $VEGF_{165}$. The fluorescence intensity of the $VEGF_{165}$/p-COF/Apt_{VEGF}/CDs system increases gradually with increasing the $VEGF_{165}$ concentration within 1.0 pg mL^{-1} to 100 ng mL^{-1}, then reaching a plateau when the $VEGF_{165}$ concentration was 200 ng mL^{-1}. It suggests the formation of an equilibrium between $VEGF_{165}$ and the aptamer strands. Thus, the determination behavior of $VEGF_{165}$ with the proposed p-COF-based fluorescent aptasensor followed the Langmuir–Freundlich isotherm [56]. The wavelength of excitation emission for the $VEGF_{165}$/p-COF/Apt_{VEGF}/CDs system shifted from 353.6 to 378.3 nm, which is close to the fluorescence performance of CDs. The fluorescence intensity (I stands the fluorescence intensity of the $VEGF_{165}$/p-COF/Apt_{VEGF}/CDs system in the presence of $VEGF_{165}$, respectively) was analyzed as a function of the logarithm of $VEGF_{165}$ concentration ($logCon_{VEGF}$). A good linear relationship was obtained between the fluorescence response signal and the $logCon_{VEGF}$ within the $VEGF_{165}$ concentration range from 1.0 pg mL^{-1} to 100 ng mL^{-1}. The calibration plot is shown as: $I = 223.29 logC_{VEGF165} + 816.62$ with the correlation coefficient (R^2) of 0.9981. On the basis of IUPAC, LOD was calculated to be 20.9 fg mL^{-1} by using the following equation: $LOD = 3\sigma/s$ (σ was the standard deviation of the corrected blank signals and s was the slope of the calibration curve). Compared with previously reported aptasensors for determination of $VEGF_{165}$ (Table 1), the fabricated p-COF-based fluorescence biosensor exhibits lower LOD and wider linear range of the $VEGF_{165}$ concentration. The outstanding sensing performance of the developed aptasensor based on p-COF nanospheres compared with other two-dimensional matrices is mainly attributed to the following aspects: (i) intrinsic cavities, three-dimensional, π-π interaction, and hydrogen bond between p-COF nanosheets facilitate the $VEGF_{165}$ aptamer immobilization [57]. (ii) The significant overlap between CDs and the emission spectra of p-COF results in the effective fluorescence quenching of the Apt_{VEGF}/CDs probe with high energy transfer efficiency. (iii) The high-specific recognition between the aptamer and $VEGF_{165}$ leads to the specific detection of $VEGF_{165}$ with low background and fast response [58].

3.5. Selectivity, stability, and regenerability of the p-COF-based fluorescence aptasensor

The selectivity of the p-COF-based fluorescence aptasensor toward $VEGF_{165}$ was further evaluated through analysis of interferents that possibly coexist with $VEGF_{165}$ in human serum. These interferences include BSA, HER2, PSA, PTK7, MUC1, CEA, AFP, typical metal ions existence in the human body including Ca^{2+}, Na^{+}, K^{+} and their mixture with $VEGF_{165}$ (100-fold that of $VEGF_{165}$, 1 μg mL^{-1}). The fluorescence response signals of each interferent and mixture are displayed in Fig. 3d. A significant change in the fluorescence signal of the $VEGF_{165}$/p-COF/Apt_{VEGF}/CDs system was observed in the presence of $VEGF_{165}$. Nonetheless, no obvious fluorescence signal was determined when detecting some proteins, other biomarkers and metal ions, only showing less than 5% of that of the detection of $VEGF_{165}$. The fluorescence signal for the detection of the mixture is higher than that of $VEGF_{165}$ determination by 7.5%. The existence of Ca^{2+}, Na^{+}, and K^{+} has no remarkable influence on the detection of biomarker $VEGF_{165}$, which is consistent with other publications [38]. All these results verify the high selectivity of the proposed p-COF-based fluorescence aptasensor toward $VEGF_{165}$. The reproducibility of the constructed fluorescence aptasensor was evaluated using five parallel p-COF-based fluorescence biosensors to detect $VEGF_{165}$ (10 ng mL^{-1}). Fig. 3e indicates no substantial variation in the relative fluorescence signals for five biosensors, indicating the relative standard deviation (RSD) of 3.6% (n = 5). This finding proves that the proposed p-COF-based fluorescence aptasensor exhibits good reproducibility. In addition, the storage stability of the p-COF-based sensor was tested by daily measuring the p-COF/Apt_{VEGF}/CDs solution toward $VEGF_{165}$ (10 ng mL^{-1}) during storage in a refrigerator at 4 °C for 15 days. As shown in Fig. 3f, the relative fluorescence signal remained 103.7% of the original signal, manifesting that the fabricated p-COF--based fluorescent aptasensor can meet long-term storage requirement.

3.6. Biocompatibility and cell images of the p-COF fluoresence aptasensor for detecting $VEGF_{165}$

Given that living MCF-7 cells are overexpressed with $VEGF_{165}$ [46], they can be determined by the present aptasensor via the binding of the

Table 1
Comparison of LOD of the p-COF-based fluorescence aptasensor with some previously reported aptasensors for detecting $VEGF_{165}$.

Materials	Methods	Detection range	LOD	Refs.
Mn-doped ZnS quantum dots	FL	0.1–16 nM	0.08 nM	[59]
ssDNA	molecular dynamics	0.01–10 ng mL^{-1}	0.005 ng mL^{-1}	[60]
graphene oxide	FL	0.5–100 nM	0.3 nM	[61]
nanogold-dot (NGD)	localized surface plasmon resonance	0.01–100 ng mL^{-1}	0.01 ng mL^{-1}	[62]
Poly T templated CuNPs	Fluorescent strategy	10–80 nM	1.3 nM	[63]
carboxyl-coated polystyrene microspheres	surface plasmon resonance (SPR)	0.1–1 ng mL^{-1}	0.1 ng mL^{-1}	[64]
p-COF	**FL**	**0.001–100 ng mL^{-1}**	**20.9 fg mL^{-1}**	**This work**

$VEGF_{165}$ aptamer to the nuclein of cells. Considering the satisfactory fluorescence performance of Apt_{VEGF}/CDs and p-COF, the present sensing system can be used to detect MCF-7 cells by using CLSM image. Prior to study of the intracellular uptake on living cells, the toxicities of p-COF and p-COF/Apt_{VEGF}/CDs were evaluated by MTT. Living MCF-7 cells and normal L929 cells were chosen to determine cell viability against p-COF and p-COF/Apt_{VEGF}/CDs (Fig. 4a and b, respectively). The viability of MCF-7 and L929 cells against p-COF is slightly higher than that of the p-COF/Apt_{VEGF}/CDs complex. Moreover, the viability of living cells decreases with increasing concentration of the p-COF and p-COF/Apt_{VEGF}/CDs suspensions. At 80 μg mL^{-1} p-COF suspension, the viability levels of MCF-7 and L929 cells are 88.1% and 85.2%, respectively, and 82.3% and 81.7% against the p-COF/Apt_{VEGF}/CDs with the same concentration. These findings suggest that p-COF and p-COF/Apt_{VEGF}/CDs display excellent biocompatibility for both cancer cells and normal cells. Hence, the proposed sensor exhibits potential for detecting living cancer cells.

Given that the excellent biocompatibility and proper size of p-COF nanospheres, the sensing performance of the constructed p-COF-based biosensor toward living MCF-7 cells using can be tested by cell images. For comparison, the cell uptake behavior of normal L929 cells was performed under the same experimental conditions. The suspensions of p-COF, Apt_{VEGF}/CDs, and p-COF/Apt_{VEGF}/CDs were incubated with the suspension of MCF-7 cells in DMEM for 1 h, for which the cell uptake images were recorded. As illustrated in Fig. 4c, no clear fluorescence of the p-COF in the CLSM image was observed against MCF-7 cells, owing to the poor target ability of the pristine p-COF toward cancer cells. For the Apt_{VEGF}/CDs complex, the weak green color in the CLSM merge image was observed, which could be due to the specific recognition between $VEGF_{165}$ that is overexpressed in the nucleolus of MCF-7 cells and the $VEGF_{165}$ aptamer. For the p-COF/Apt_{VEGF}/CDs complex incubated with the suspension of MCF-7 cells, brighter green color was found. As known, the p-COF/Apt_{VEGF}/CDs complex can be absorbed by MCF-7 cells due to the specific recognition between the aptamer and MCF-7 cells. Afterward, the Apt_{VEGF}/CDs complex can be released from the p-COF matrix, resulting in the recovery of the fluorescence, which can be determined using the CLSM image. By contrast, no apparent fluorescence signal was observed in the sensing system when incubated with the suspension of L929 cells (Fig. S5). Given the low level of $VEGF_{165}$ in L929 cells, no specific adsorption of all nanomaterials occurred within cells. Hence, the proposed p-COF-based fluorescence aptasensor not can be used not only to detect $VEGF_{165}$ in aqueous solution but also to directly determine living cancer cells.

In comparison with other fluorescence sensors, the aptasensor based on p-COF and biocompatible CDs demonstrates following advantages. (i) The $VEGF_{165}$-targeted aptamer labeled with amino group can be strongly anchored onto the carboxyl group-functionalized CDs via covalent bond of N–C═O, stronger than the interaction between CDs and p-COFs. It thus ensures the release of the Apt_{VEGF}/CDs complex from the p-COF rather than individually falling off. (ii) The three-dimensional network, porous nanostructure, and intrinsic cavities of p-COF along with the residual amino groups lead to the efficient adsorption of the Apt_{VEGF}/CDs complex, boosting the detection sensitivity. Furthermore, the proposed aptasensor exhibits good detection sensitivity also due to the well matching between the fluorescence performance of CDs and p-COF compared with other conventional CD and adsorption matrix. (iii) The excellent fluorescence of p-COF and CDs efforts the developed aptasensor with the feasibility and bifunctional sensing performances for detection of $VEGF_{165}$ and living cancer cells. Hence, the proposed p-COF-based fluorescence biosensor shows potential for early diagnosis of various cancer markers when immobilizing other kinds of aptamers.

3.7. Real samples

The p-COF/Apt_{VEGF}/CDs aptasensor was used to detect human serum samples obtained from the First Affiliated Hospital of Zhengzhou University to evaluate the practicability for clinical diagnosis. $VEGF_{165}$ solutions with different concentrations were spiked into human serum. Theoretical $VEGF_{165}$ concentrations were deduced according to the regression equation (Fig. 3c) and compared with the practical spike value. As shown in Table S1, high recoveries of 94.1%–106.4% and small RSDs (less than 5%) were obtained, suggesting the application prospects of the proposed p-COF-based fluorescence aptasensor.

4. Conclusion

We report a general strategy for fabricating a fluorescence-based aptasensor by using p-COF nanospheres as a sensitive scaffold to detect $VEGF_{165}$ and living MCF-7 cells. The as-synthesized p-COF exhibited exceptional stability, intrinsic cavities, strong fluorescence, and good biocompatibility, thereby indicating the high stability and adsorption capability of the aptamer. The p-COF was suitable for development of fluorescence biosensors. The fluorescence of the proposed biosensor was initially quenched due to the efficient FRET effect between the p-COF matrix and the Apt_{VEGF}/CDs. As such, a turn-on signal was sequentially observed upon the addition of $VEGF_{165}$. The proposed biosensor exhibited ultrahigh sensitivity, with a detection limit of 20.9 fg mL^{-1} within a wide $VEGF_{165}$ concentration range of 1.0 pg mL^{-1}–100 ng mL^{-1}. The applicability of the fluorescence biosensor for real sample analysis was demonstrated by probing $VEGF_{165}$ spiked in human serum samples. The proposed p-COF-based aptasensor was explored for detecting MCF-7 cells overexpressing $VEGF_{165}$ by cell imaging technique. Moreover, the ultrasensitive detection of other analytes was achieved by simply changing the specific target recognition substrate. The sensor could be used as a versatile fluorescence platform for ultrasensitive detection of various biomarkers. Therefore, the proposed fluorescence biosensor has great potential to be applied in bioanalysis and clinical biomedicine.

Author statement

Jing Cui: Validation, Formal Analysis, Writing-Original Draft. Lun Kan, Zhenzhen Li: Validation, Formal Analysis. Longyu Yang: Formal Analysis, Investigation. Minghua Wang: Conceptualization, Writing - Review & Editing. Linghao He: Methodology, Formal Analysis. Yafei Lou: Writing - Review & Editing, Supervision. Zhihong Zhang: Validation, Formal Analysis, Review & Editing, Supervision.

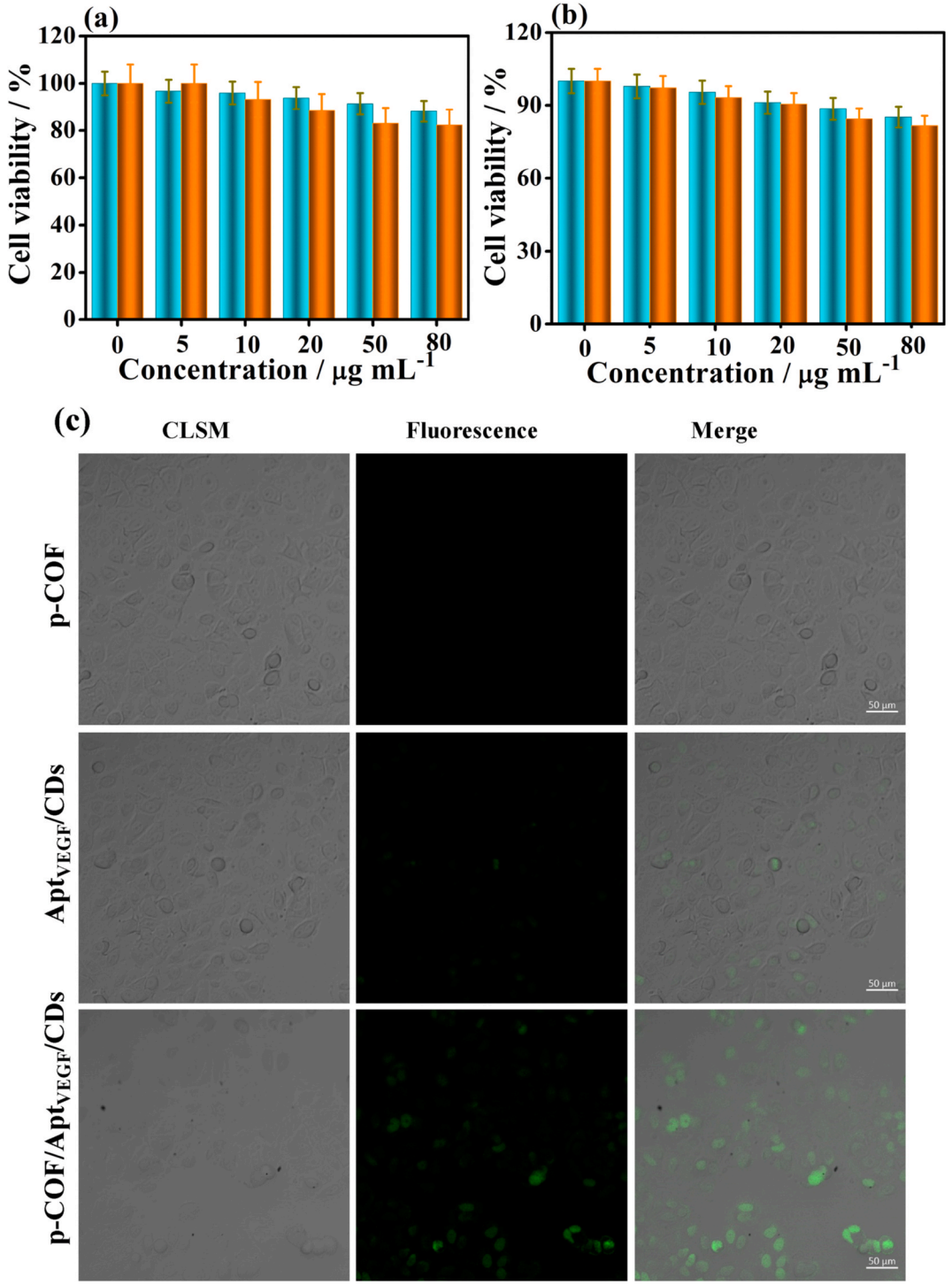

Fig. 4. Cell viabilities of p-COF (green column) and p-COF/CDs/Apt$_{VEGF}$/VEGF (brown column) for (a) MCF-7 cancer cells and (b) L929 normal cells (8000 cells well^{-1}), respectively. (c) Fluorescence images of p-COF, Apt$_{VEGF}$/CDs, and p-COF/Apt$_{VEGF}$/CDs incubated with the suspension of living MCF-7 cells (1×10^5 cells well^{-1}) for 1 h excited by 370 nm laser. (For interpretation of the references to color in this figure legend, the reader is referred to the Web version of this article.)

Declaration of competing interest

We declare that we have no conflict of interest.

Acknowledgment

This work was supported by the Outstanding Youth Science Fund Project of Henan (CN) (No. 202300410492), the National Natural Science Foundation of China (No. 51903224), and the Key Project of University in Henan Province (18A43004).

Appendix A. Supplementary data

Supplementary data to this article can be found online at https://doi.org/10.1016/j.talanta.2020.122060.

References

[1] N. Zhou, F. Su, C. Guo, L. He, Z. Jia, M. Wang, Q. Jia, Z. Zhang, S. Lu, Two-dimensional oriented growth of Zn-MOF-on-Zr-MOF architecture: a highly sensitive and selective platform for detecting cancer markers, Biosens. Bioelectron. (123) (2019) 51–58, https://doi.org/10.1016/j.bios.2018.09.079.

[2] C. Gu, C. Guo, Z. Li, M. Wang, N. Zhou, L. He, Z. Zhang, M. Du, Bimetallic ZrHf-based metal-organic framework embedded with carbon dots: ultra-sensitive platform for early diagnosis of HER2 and HER2-overexpressed living cancer cells, Biosens. Bioelectron. 134 (2019) 8–15, https://doi.org/10.1016/j.bios.2019.03.043.

[3] Y. Wang, J. Luo, J. Liu, S. Sun, Y. Xiong, Y. Ma, S. Yan, Y. Yang, H. Yin, X. Cai, Label-free microfluidic paper-based electrochemical aptasensor for ultrasensitive and simultaneous multiplexed detection of cancer biomarkers, Biosens. Bioelectron. (136) (2019) 84–90, https://doi.org/10.1016/j.bios.2019.04.032.

[4] Y. Li, M. Hu, X. Huang, M. Wang, L. He, Y. Song, Q. Jia, N. Zhou, Z. Zhang, M. Du, Multicomponent zirconium-based metal-organic frameworks for impedimetric aptasensing of living cancer cells, Sens. Actuators B-Chem. (306) (2020) 127608, https://doi.org/10.1016/j.snb.2019.127608.

[5] H. Xiong, J. Yan, S. Cai, Q. He, D. Peng, Z. Liu, Y. Liu, Cancer protein biomarker discovery based on nucleic acid aptamers, Int. J. Biol. Macromol. (132) (2019) 190–202, https://doi.org/10.1016/j.ijbiomac.2019.03.165.

[6] H. Da, H. Liu, Y. Zheng, R. Yuan, Y. Chai, A highly sensitive VEGF165 photoelectrochemical biosensor fabricated by assembly of aptamer bridged DNA networks, Biosens. Bioelectron. (101) (2018) 213–218, https://doi.org/10.1016/j.bios.2017.10.032.

[7] R.M.B. Loureiro, P.A. D'Amore, Transcriptional regulation of vascular endothelial growth factor in cancer, Cytokine Growth Factor Rev. 1 (16) (2005) 77–89, https://doi.org/10.1016/j.cytogfr.2005.01.005.

[8] L. Pan, S. Kuo, T. Lin, C. Lin, P. Fang, H. Yang, An electrochemical biosensor to simultaneously detect VEGF and PSA for early prostate cancer diagnosis based on graphene oxide/ssDNA/PLLA nanoparticles, Biosens. Bioelectron. (89) (2017) 598–605, https://doi.org/10.1016/j.bios.2016.01.077.

[9] F.M. Moghadam, M. Rahaie, A signal-on nanobiosensor for $VEGF_{165}$ detection based on supraparticle copper nanoclusters formed on bivalent aptamer, Biosens. Bioelectron. (132) (2019) 186–195, https://doi.org/10.1016/j.bios.2019.02.046.

[10] J.E. Park, G.A. Keller, N. Ferrara, The vascular endothelial growth factor (VEGF) isoforms: differential deposition into the subepithelial extracellular matrix and bioactivity of extracellular matrix-bound VEGF, Mol. Biol. Cell 12 (4) (1993) 1317–1326, https://doi.org/10.1091/mbc.4.12.1317.

[11] H. Takahashi, Y. Nomura, J. Nishida, Y. Fujino, Y. Yanagi, H. Kawashima, Vascular endothelial growth factor (VEGF) concentration is underestimated by enzyme-linked immunosorbent assay in the presence of anti-VEGF drugs VEGF ELISA concentration with inhibitors present, Invest. Ophthalmol. Vis. Sci. 2 (57) (2016) 462–466, https://doi.org/10.1167/iovs.15-18245.

[12] V. Goncalves, B. Gautier, C. Garbay, M. Vidal, N. Inguimbert, Development of a chemiluminescent screening assay for detection of vascular endothelial growth factor receptor 1 ligands, Anal. Biochem. 1 (366) (2007) 108–110, https://doi.org/10.1016/j.ab.2007.03.027.

[13] V.K. Gupta, A.K. Singh, L.K. Kumawat, Thiazole Schiff base turn-on fluorescent chemosensor for Al^{3+} ion, Sensor. Actuator. B Chem. (195) (2014) 98–108, https://doi.org/10.1016/j.snb.2013.12.092.

[14] V.K. Gupta, N. Mergu, L.K. Kumawat, A.K. Singh, Selective naked-eye detection of Magnesium (II) ions using a coumarin-derived fluorescent probe, Sensor. Actuator. B Chem. (207) (2015) 216–223, https://doi.org/10.1016/j.snb.2014. 10.044.

[15] V.K. Gupta, N. Mergu, L.K. Kumawat, A.K. Singh, A reversible fluorescence "off-on-off" sensor for sequential detection of aluminum and acetate/fluoride ions, Talanta 144 (2015) 80–89, https://doi.org/10.1016/j.talanta.2015.05.053.

[16] H. Cho, E.-C. Yeh, R. Sinha, T.A. Laurence, J.P. Bearinger, L.P. Lee, Single-step nanoplasmonic $VEGF_{165}$ aptasensor for early cancer diagnosis, ACS Nano 9 (6) (2012) 7607–7614, https://doi.org/10.1021/nn203833d.

[17] H. Zhang, M. Li, C. Li, Z. Guo, H. Dong, P. Wu, C. Cai, G-quadruplex DNAzyme-based electrochemiluminescence biosensing strategy for $VEGF_{165}$ detection: combination of aptamer-target recognition and T7 exonuclease-assisted cycling signal amplification, Biosens. Bioelectron. (74) (2015) 98–103, https://doi.org/10.1016/j.bios.2015.05.069.

[18] R.Y. Lai, K.W. Plaxco, A.J. Heeger, Aptamer-based electrochemical detection of picomolar platelet-derived growth factor directly in blood serum, Anal. Chem. 1 (79) (2007) 229–233, https://doi.org/10.1021/ac061592s.

[19] S. Zhao, W. Yang, R. Lai, A folding-based electrochemical aptasensor for detection of vascular endothelial growth factor in human whole blood, Biosens. Bioelectron. 5 (26) (2011) 2442–2447, https://doi.org/10.1016/j.bios.2010.10. 029.

[20] K. Kopra, M. Syrjänpää, P. Hänninen, H. Härmä, Non-competitive aptamer-based quenching resonance energy transfer assay for homogeneous growth factor quantification, Analyst 8 (139) (2014) 2016–2023, https://doi.org/10.1039/C3AN01814H.

[21] R. Freeman, J. Girsh, A. Fang Jou, J.A. Ho, T. Hug, J. Dernedde, I. Willner, Optical aptasensors for the analysis of the vascular endothelial growth factor (VEGF), Anal. Chem. 14 (84) (2012) 6192–6198, https://doi.org/10.1021/ac3011473.

[22] S. Shoora, A. Jain, V. Gupta, A simple Schiff base based novel optical probe for aluminium (III) ions, Sensor. Actuator. B Chem. (216) (2015) 86–104, https://doi.org/10.1016/j.snb.2015.04.038.

[23] Z. Qian, X. Shan, L. Chai, J. Ma, J. Chen, H. Feng, DNA nanosensor based on biocompatible graphene quantum dots and carbon nanotubes, Biosens. Bioelectron. (60) (2014) 64–70, https://doi.org/10.1016/j.bios.2014.04.006.

[24] W. Algar, U. Krull, Toward a multiplexed solid-phase nucleic acid hybridization assay using quantum dots as donors in fluorescence resonance energy transfer, Anal. Chem. 10 (81) (2009) 4113–4120, https://doi.org/10.1021/ac900421p.

[25] C. Zhang, J. Hu, Single quantum dot-based nanosensor for multiple dna detection, Anal. Chem. 5 (82) (2010) 1921–1927, https://doi.org/10.1021/ac9026675.

[26] J. Shi, C. Chan, Y. Pang, W. Ye, F. Tian, J. Lyu, Y. Zhang, M. Yang, A fluorescence resonance energy transfer (FRET) biosensor based on graphene quantum dots (GQDs) and gold nanoparticles (AuNPs) for the detection of mecA gene sequence of Staphylococcus aureus, Biosens. Bioelectron. 67 (2015) 595–600, https://doi.org/10.1016/j.bios.2014.09.059.

[27] X. Zheng, A. Ananthanarayanan, K. Luo, P. Chen, Glowing graphene quantum dots and carbon dots: properties, syntheses, and biological applications, Small 14 (11) (2015) 1620–1636, https://doi.org/10.1002/smll.201402648.

[28] L. Cao, X. Wang, M. Meziani, F. Lu, H. Wang, P. Luo, Y. Lin, B. Harruff, L. Veca, D. Murray, S. Xie, Y. Sun, Carbon dots for multiphoton bioimaging, J. Am. Chem. Soc. 37 (129) (2007) 11318–11319, https://doi.org/10.1021/ja073527l.

[29] H. Babu, M. Bai, M. Rajeswara Rao, Functional π-conjugated two-dimensional covalent organic frameworks, ACS Appl. Mater. Interfaces 12 (11) (2019) 11029–11060, https://doi.org/10.1021/acsami.8b19087.

[30] N. Keller, M. Calik, D. Sharapa, H. Soni, P. Zehetmaier, S. Rager, F. Auras, A. Jakowetz, A. Görling, T. Clark, T. Bein, Enforcing extended porphyrin J-aggregate stacking in covalent organic frameworks, J. Am. Chem. Soc. 48 (140) (2018) 16544–16552, https://doi.org/10.1021/jacs.8b08088.

[31] X. Feng, X. Ding, D. Jiang, Covalent organic frameworks, Chem. Soc. Rev. 18 (41) (2012) 6010–6022, https://doi.org/10.1039/C2CS35157A.

[32] N. Huang, P. Wang, D. Jiang, Covalent organic frameworks: a materials platform for structural and functional designs, Nat. Mater. 10 (1) (2016) 16068, https://doi.org/10.1038/natrevmats.2016.68.

[33] J.L. Segura, M.J. Mancheño, F. Zamora, Covalent organic frameworks based on Schiff-base chemistry: synthesis, properties and potential applications, Chem. Soc. Rev. 20 (45) (2016) 5635–5671, https://doi.org/10.1039/C5CS00878F.

[34] X. Zhang, K. Chi, D. Li, Y. Deng, Y. Ma, Q. Xu, R. Hu, Y. Yang, 2D-porphrinic covalent organic framework-based aptasensor with enhanced photoelectrochemical response for the detection of C-reactive protein, Biosens. Bioelectron. (129) (2019) 64–71, https://doi.org/10.1016/j.bios.2019.01.009.

[35] M. Wang, M. Hu, J. Liu, C. Guo, D. Peng, Q. Jia, L. He, Z. Zhang, M. Du, Covalent organic framework-based electrochemical aptasensors for the ultrasensitive detection of antibiotics, Biosens. Bioelectron. (132) (2019) 8–16, https://doi.org/10.1016/j.bios.2019.02.040.

[36] M. Xu, L. Wang, Y. Xie, Y. Song, L. Wang, Ratiometric electrochemical sensing and biosensing based on multiple redox-active state COFDHTA-TTA, Sensor. Actuator. B Chem. (281) (2019) 1009–1015, https://doi.org/10.1016/j.snb.2018. 11.032.

[37] W. Li, C. Yang, X. Yan, A versatile covalent organic framework-based platform for sensing biomolecules, Chem. Commun. (J. Chem. Soc. Sect. D) 83 (53) (2017) 11469–11471, https://doi.org/10.1039/C7CC06244C.

[38] S. Ding, M. Dong, Y. Wang, Y. Chen, H. Wang, C. Su, W. Wang, Thioether-based fluorescent covalent organic framework for selective detection and facile removal of mercury(II), J. Am. Chem. Soc. 9 (138) (2016) 3031–3037, https://doi.org/10.1021/jacs.5b10754.

[39] C. Zhang, S. Zhang, Y. Yan, F. Xia, A. Huang, Y. Xian, Highly fluorescent polyimide covalent organic nanosheets as sensing probes for the detection of 2,4,6-trinitrophenol, ACS Appl. Mater. Interfaces 15 (9) (2017) 13415–13421, https://doi.org/10.1021/acsami.6b16423.

[40] C. Yuan, B. Liu, F. Liu, M. Han, Z. Zhang, Fluorescence "turn on" detection of mercuric ion based on bis(dithiocarbamato)copper(ii) complex functionalized carbon nanodots, Anal. Chem. 2 (86) (2014) 1123–1130, https://doi.org/10.1021/ac402894z.

[41] A. Akthakul, N. Maklakov, J. White, Improved vapor sensitivity by rationally designing fluorescent turn-on sensors, Anal. Chem. 15 (82) (2010) 6487–6494, https://doi.org/10.1021/ac1007859.

[42] Y. Zhao, F. Zheng, W. Ke, W. Zhang, L. Shi, H. Liu, Gap-tethered Au@AgAu Raman tags for the ratiometric detection of MC-LR, Anal. Chem. 11 (91) (2019) 7162–7172, https://doi.org/10.1021/acs.analchem.9b00348.

[43] Y. Peng, Y. Huang, Y. Zhu, B. Chen, L. Wang, Z. Lai, Z. Zhang, M. Zhao, C. Tan, N. Yang, F. Shao, Y. Han, H. Zhang, Ultrathin two-dimensional covalent organic framework nanosheets: preparation and application in highly sensitive and selective DNA detection, J. Am. Chem. Soc. 25 (139) (2017) 8698–8704, https://doi.org/10.1021/jacs.7b04096.

[44] Z. Zhang, S. Zhang, L. He, D. Peng, F. Yan, M. Wang, J. Zhao, H. Zhang, S. Fang, Feasible electrochemical biosensor based on plasma polymerization-assisted composite of polyacrylic acid and hollow TiO_2 spheres for sensitively detecting lysozyme, Biosens. Bioelectron. (74) (2015) 384–390, https://doi.org/10.1016/j.bios. 2015.06 .062.

[45] X. Gao, B. Zhang, Q. Zhang, Y. Tang, X. Liu, J. Li, The influence of combination mode on the structure and properties of graphene quantum dot-porphyrin composites, Colloids Surf. B Biointerfaces (172) (2018) 207–212, https://doi.org/10.1016/j.colsurfb.2018.08.010.

[46] H. Bawadi, R. Bansode, A. Trappey, R. Truax, J. Losso, Inhibition of Caco-2 colon, MCF-7 and Hs578T breast, and DU 145 prostatic cancer cell proliferation by water-soluble black bean condensed tannins, Canc. Lett. 2 (218) (2005) 153–162, https://doi.org/10.1016/j.canlet.2004.06.021.

[47] S. Wan, F. Gándara, A. Asano, H. Furukawa, A. Saeki, S.K. Dey, L. Liao, M. W. Ambrogio, Y.Y. Botros, X. Duan, S. Seki, J.F. Stoddart, O.M. Yaghi, Covalent organic frameworks with high charge carrier mobility, Chem. Mater. 18 (23) (2011) 4094–4097, https://doi.org/10.1021/cm201140r.

[48] M. Guo, J. Chen, D. Liu, L. Nie, S. Yao, Electrochemical characteristics of the immobilization of calf thymus DNA molecules on multi-walled carbon nanotubes, Bioelectrochemistry 1 (62) (2004) 29–35, https://doi.org/10.1016/j. bioelechem.2003.10.005.

[49] J. Yoo, S. Lee, S. Hirata, C. Kim, C.K. Lee, T. Shiraki, N. Nakashima, J.K. Shim, In situ synthesis of covalent organic frameworks (COFs) on carbon nanotubes and graphenes by sonochemical reaction for CO_2 adsorbents, Chem. Lett. 4 (44) (2015) 560–562, https://doi.org/10.1246/cl.141194.

[50] H. Li, C. Wang, T. Hou, F. Li, Amphiphile-mediated ultrasmall aggregation induced emission dots for ultrasensitive fluorescence biosensing, Anal. Chem. 17 (89) (2017) 9100–9107, https://doi.org/10.1021/acs.analchem.7b01797.

[51] K. Artyushkova, J.O. Farrar, J.E. Fulghum, Data fusion of XPS and AFM images for chemical phase identification in polymer blends, Surf. Interface Anal. 2 (41) (2009) 119–126, https://doi.org/10.1002/sia.2968.

[52] J. Qian, H. Cui, X. Lu, C. Wang, K. An, N. Hao, K. Wang, Bi-color FRET from two nano-donors to a single nano-acceptor: a universal aptasensing platform for simultaneous determination of dual targets, Chem. Eng. J. (401) (2020) 126017, https://doi.org/10.1016/j.cej.2020.126017.

[53] X. Yan, Y. Song, J. Liu, N. Zhou, C. Zhang, L. He, Z. Zhang, Z. Liu, Two-dimensional porphyrin-based covalent organic framework: a novel platform for sensitive epidermal growth factor receptor and living cancer cell detection, Biosens. Bioelectron. (126) (2019) 734–742, https://doi.org/10.1016/j.bios.2018. 11.047.

[54] Z. Li, Y. Zhang, H. Xia, Y. Mu, X. Liu, A robust and luminescent covalent organic framework as a highly sensitive and selective sensor for the detection of Cu^{2+} ions, Chem. Commun. (J. Chem. Soc. Sect. D) 39 (52) (2016) 6613–6616, https://doi.org/10.1039/C6CC01476C.

[55] Z. Zhou, X. Zhang, L. Xing, J. Liu, A. Kong, Y. Shan, Copper-assisted thermal conversion of microporous covalent melamine-boroxine frameworks to hollow B, N-codoped carbon capsules as bifunctional metal-free electrode materials, Electrochim. Acta 298 (2019) 210–218, https://doi.org/10.1016/j.electacta.2018.12.080.

[56] M. Wang, M. Hu, Z. Li, L. He, Y. Song, Q. Jia, Z. Zhang, M. Du, Construction of Tb-MOF-on-Fe-MOF conjugate as a novel platform for ultrasensitive detection of carbohydrate antigen 125 and living cancer cells, Biosens, Bioelectron 142 (2019) 111536, https://doi.org/10.1016/j.bios.2019.111536.

[57] D. Jiang, T. Hu, H. Zheng, G. Xu, Q. Jia, Aptamer-functionalized magnetic conjugated organic framework for selective extraction of traces of hydroxylated polychlorinated biphenyls in human serum, Chem. Eur J. 41 (24) (2018) 10390–10396, https://doi.org/10.1002/chem.201800092.

[58] X. Lin, K. Leung, L. Lin, L. Lin, S. Lin, C. Leung, D. Ma, J. Lin, Determination of cell metabolite $VEGF_{165}$ and dynamic analysis of protein-DNA interactions by combination of microfluidic technique and luminescent switch-on probe, Biosens. Bioelectron. (79) (2016) 41–47, https://doi.org/10.1016/j.bios.2015.11.089.

[59] D. Zhu, W. Li, H.-M. Wen, S. Yu, Z. Miao, A. Kang, A. Zhang, Silver nanoparticles-enhanced time-resolved fluorescence sensor for $VEGF_{165}$ based on Mn-doped ZnS quantum dots, Biosens. Bioelectron. (74) (2015) 1053–1060, https://doi.org/10.1016/j.bios.2015.08.005.

[60] B. Çakıroğlu, M. Özacar, A self-powered photoelectrochemical glucose biosensor based on supercapacitor Co_3O_4-CNT hybrid on TiO_2, Biosens. Bioelectron. 119 (2018) 34–41, https://doi.org/10.1016/j.bios.2018.07.049.

[61] J. Xu, W. Chen, M. Shi, Y. Huang, L. Fang, S. Zhao, L. Yao, H. Liang, An aptamer-based four-color fluorometic method for simultaneous determination and imaging of alpha-fetoprotein, vascular endothelial growth factor-165, carcinoembryonic antigen and human epidermal growth factor receptor 2 in living cells, Microchim, Acta 3 (186) (2019) 204, https://doi.org/10.1007/s00604-019-3312-1.

[62] H. Yang, R. Tsai, J. Chen, S. Ju, J. Liao, K. Wei, W. Zou, M. Hua, Fabrication of a nanogold-dot array for rapid and sensitive detection of vascular endothelial growth factor in human serum, ACS Appl. Mater. Interfaces 45 (8) (2016) 30845–30852, https://doi.org/10.1021/acsami.6b13329.

[63] Y. Cao, Z. Wang, J. Cao, X. Mao, G. Chen, J. Zhao, A general protein aptasensing strategy based on untemplated nucleic acid elongation and the use of fluorescent copper nanoparticles: application to the detection of thrombin and the vascular endothelial growth factor, Microchim. Acta 10 (184) (2017) 3697–3704, https://doi.org/10.1007/s00604-017-2393-y.

[64] H. Chen, Y. Hou, F. Qi, J. Zhang, K. Koh, Z. Shen, G. Li, Detection of vascular endothelial growth factor based on rolling circle amplification as a means of signal enhancement in surface plasmon resonance, Biosens. Bioelectron. (61) (2014) 83–87, https://doi.org/10.1016/j.bios.2014.05.005.